Probabilistic Fringe-fitting and Source Model Comparison

Iniyan Natarajan
Rhodes University / South African Radio Astronomy Observatory (SARAO)

with Roger Deane, Zsolt Paragi, Ilse van Bemmel, Des Small, Huib Jan van Langevelde, Mark Kettenis, Oleg Smirnov, and Arpad Szomoru

14th EVN Symposium & Users Meeting (Oct 2018, Granada)

Probability Theory for Scientific Inference

Most scientific questions fall under the category of inverse problems, in which one is required to infer causes from data in the face of incomplete information.

No unique solution exists and so additional constraints must be imposed (i.e. regularisation) to select the most plausible cause that explains the data.

This can be achieved by introducing any available prior information about the problem while drawing inferences.

Probability theory provides a mathematically consistent way of doing this by using Bayes' theorem to update one's beliefs about propositions as more information becomes available.

Bayes' Theorem

Probability is interpreted as the degree of belief in a proposition:

$$\mathcal{P}(A|B, I) = \frac{\mathcal{P}(A|I)\,\mathcal{P}(B|A, I)}{\mathcal{P}(B|I)}$$

Two levels of inference:

1. Parameter estimation: Assume that a model/hypothesis is true and estimate its parameters.
2. Model Selection: Determine the relative probabilities of alternative hypotheses given the data (i.e. visibilities).

Why visibilities?

Statistical visibility analysis complements and, if applied judiciously, can improve on traditional imaging and deconvolution.

- Measurements are made in the visibility domain.
- Imaging is difficult
  - for interferometers with sparse *uv*-coverage.
  - when the instrumental calibration is poor.
- Biased parameter and inadequate uncertainty estimates.
- Estimating errors
  - Visibility measurements are mostly independent and Gaussian.
  - Fourier transform correlates systematic errors that are localised in the *uv*-domain.
- An image is one possible realisation out of many.

Software Used

- MEQSILHOUETTE (Blecher et al., 2017) for generating synthetic EHT data.
  - Now in version v0.7 (not public yet).
  - Tropospheric corruptions.
  - Bandpass effects and other gains.
  - Full Stokes, time-variable-sky simulations.
- MONTBLANC, a GPU-implementation of the RIME, to facilitate fast model computation (Perkins et al., 2015).
  - Implemented in Python with a numpy-like API.
  - Available at https://github.com/ska-sa/montblanc.
- MULTINEST (Feroz & Hobson, 2008), and, more recently, POLYCHORD (Handley et al., 2015), for computing the posteriors and the Bayesian evidence.
  - User-written functions for prior and likelihood computation.

Fringe-fitting in VLBI

The stations participating in a VLBI observation are typically located hundreds of kilometres apart.

The atmospheric conditions at the individual stations are different, leading to different propagation delays that are uncorrelated (Thompson et al., 2017, Chapter 9).

These errors, if not corrected for, may decohere the signal completely in the worst case or reduce the coherence time, resulting in a net loss of amplitude (Schwab & Cotton, 1983).

Many subtle effects such as the atmosphere, errors in antenna and source positions are accounted for by the correlator model.

The residual variation in phases with respect to time and frequency, the rates and the delays respectively, along with constant phase offsets, are corrected using fringe-fitting.

Fringe-fitting in VLBI

Interferometer phase error, to a first order (Cotton, 1995):

$$\Delta\phi_{t,\nu} = \phi_0 + \left(\frac{\partial \phi}{\partial \nu} \Delta\nu + \frac{\partial \phi}{\partial t} \Delta t \right),$$

where ϕ_0 is the phase error at the reference time and frequency, $\frac{\partial \phi}{\partial \nu}$ is the delay residual, and $\frac{\partial \phi}{\partial t}$, the rate residual.

Simultaneously incorporate source structure in the models.

Here, we compare our method with the fringe-fitting tasks in CASA and AIPS on synthetic EHT observations of the following sky models:

- Central Gaussian source (GAU).
- Central dominant point source with a secondary point source away from the phase centre (2PT).

The RIME Used for the Inference

Accounting for the phase offsets and delays, the RIME used for the likelihood computation becomes

$$\mathbf{V}_{pq} = G_p \, \mathbf{X}_{pq} \, G_q^H + \mathcal{N}(0, \sigma_{pq}^2)$$

where G_p are the Jones matrices given by

$$G_p = \mathrm{e}^{i[\psi_p + \tau_p(\nu_n - \nu_{\mathrm{ref}})]} \begin{pmatrix} 1 & 0 \\ 0 & 1 \end{pmatrix}$$

$\mathbf{X}_{pq}$ is the source coherency matrix, and
$\mathcal{N}(0, \sigma_{pq}^2)$ is the additive noise per vis., with σ_{pq} given by the radiometer equation

$$\sigma_{pq} = \frac{\sqrt{\mathrm{SEFD}_p \, \mathrm{x} \, \mathrm{SEFD}_q}}{\sqrt{2 \delta\nu \, \tau}}$$

where $\delta\nu$ is the bandwidth and τ is the integration time.

The EHT is a network of mm/sub-mm facilities spread across continents to create a telescope with high angular resolution ($\simeq 30 - 10\,\mu$as, operating at frequencies $230 - 345$ GHz), with the longest baselines spanning the Earth's diameter (Doeleman et al. (2009)).

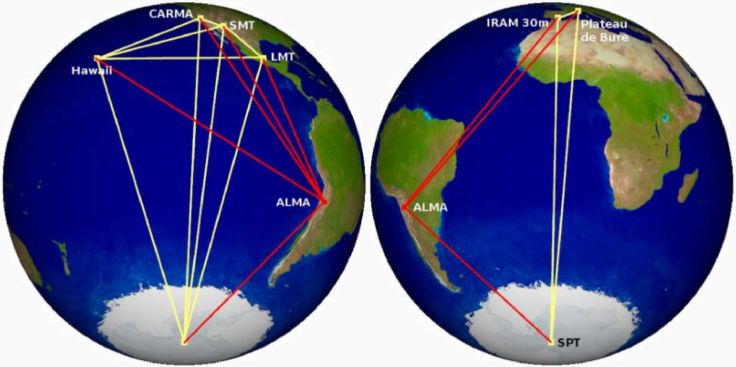

Synthetic EHT Observations (GAU)

Details of the simulations:

- 0 to 20 µas central Gaussian sources (I_p, m_p, e_{min}/e_{maj}).
- 3 minute snapshot observations.
- 2 second integration time.
- 230 GHz frequency.
- 32 channels of 80 MHz each (2.56 GHz bandwidth).

Synthetic EHT Observations (GAU)

Details of the simulations:

- SEFD-derived Gaussian thermal noise.
- Delays constant in time (3 min “solint”).
- No tropospheric turbulence.
- Comparison with FRINGEFIT (CASA) and FRING (AIPS).

Bayesian Inference

Uniform priors for the source parameters and delays.

Bayesian model selection between GAU and PT (a point source model) performed on each dataset (from 0 to 20 μas sources).

GAU was preferred in each Gaussian case with accurate estimates of the source size and instrumental delays.

Compared the posterior distributions with the estimates returned by FRINGEFIT (CASA) and FRING (AIPS).

Bayesian Inference - Posteriors for 20 µas GAU Source

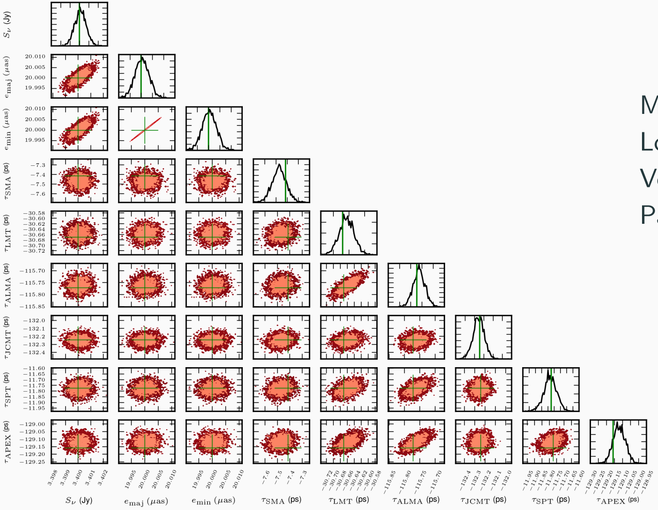

Main diagonal: 1-D posteriors

Lower triangle: 2-D correlations

Vertical green lines: simulated values

Parameters plotted:

- Flux Density, S_ν
- Major axis of Gaussian, e_{maj}
- Minor axis of Gaussian, e_{min}
- Delays, τ_p

Comparison of Delay Estimates with CASA (GAU)

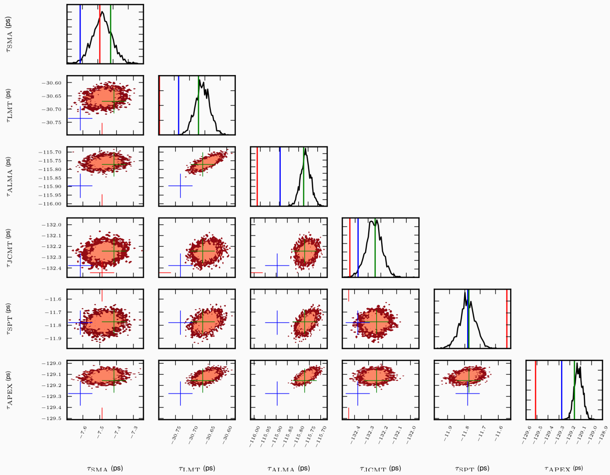

CASA estimates of delays

- Red: Point source model.
- Blue: Perfect source model.
- Green: True values.

Deriving Uncertainties for CASA Estimates (GAU)

200 simulations of the 20 μas source with the same noise properties $\mathcal{N}(\mu, \sigma)$ but different noise realisations, with and without incorporating the true sky model.

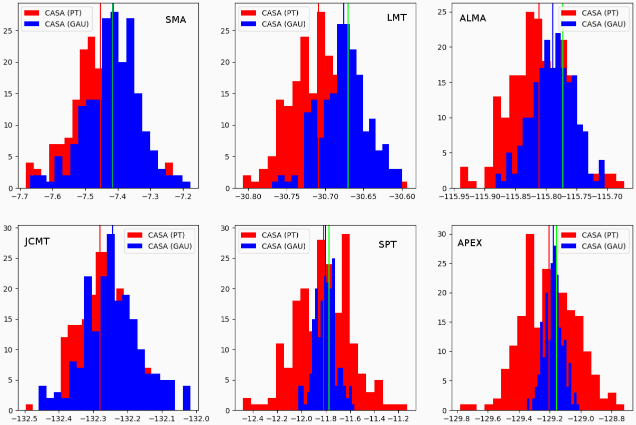

Comparison with AIPS Task FRING (performed by Ilse van Bemmel)

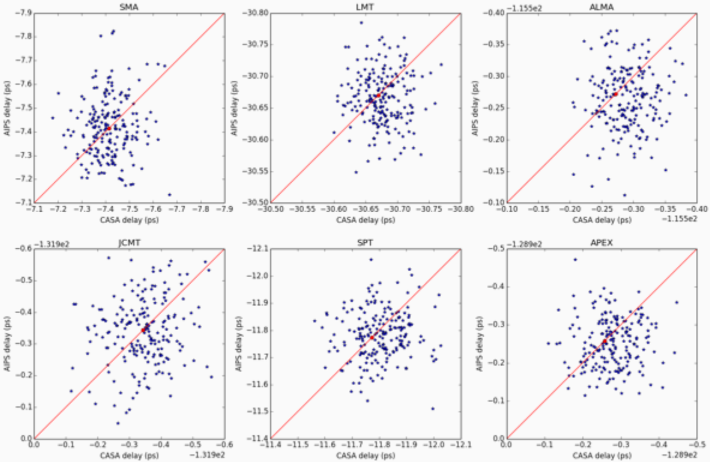

Synthetic EHT Observations (2PT)

Details of the simulations:

- Central dominant point source (1 Jy).
- 10 datasets with the secondary point source (0.3 Jy) located at distances of 10 to 100 µas in DEC, in steps of 10 µas.
- 3 minute snapshot observations.
- 2 second integration time.
- 230 GHz frequency.
- 32 channels of 80 MHz each (2.56 GHz bandwidth).
- SEFD-derived Gaussian thermal noise.
- Delays constant in time (3 min “solint”).

Bayesian Inference - Posteriors for 2PT separated by 100 μas

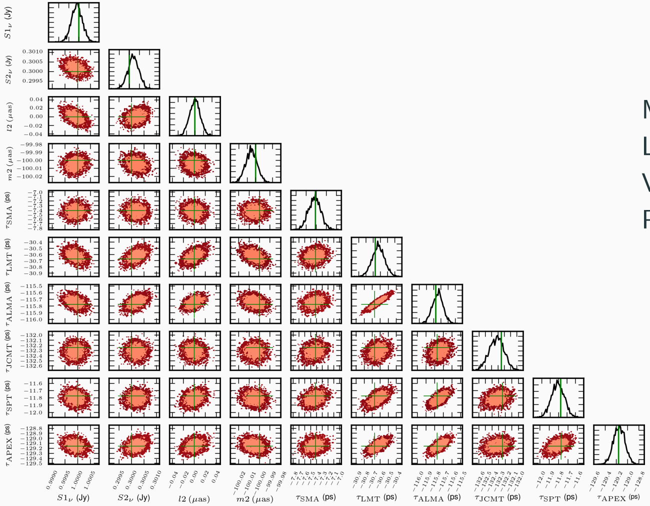

Main diagonal: 1-D posteriors

Lower triangle: 2-D correlations

Vertical green lines: simulated values

Parameters plotted:

- Flux Densities: $S_{\nu 1}$ and $S_{\nu 2}$
- Position of secondary source: (l_2, m_2)
- Delays, τ_p

Comparison of Delay Estimates with CASA (2PT)

200 simulations with the same noise properties $\mathcal{N}(\mu, \sigma)$ but different noise realisations, with and without incorporating the true sky model.

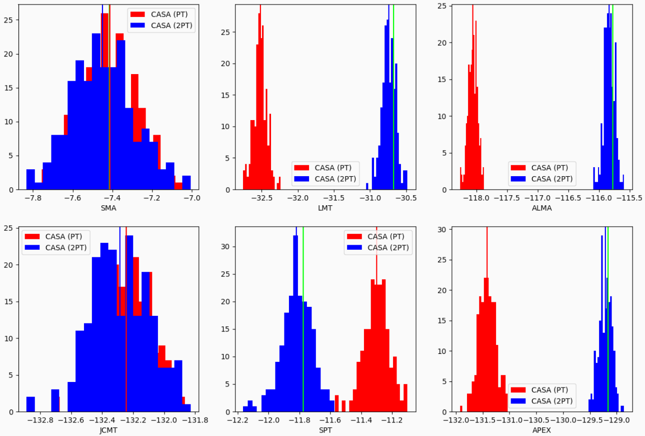

Discussion

FRINGEFIT and FRING results coincide with the posterior distributions of the parameters when the source model is incorporated during fringe-fitting.

With the point source assumption, the CASA estimates have a larger spread and/or differ from the actual delays by a few picoseconds.

For wideband observations at high frequencies, with more complex source models, we may expect these differences to become more significant (need to be sure not to “burn in” these discrepancies).

The Bayesian estimates provide tight constraints on the posteriors, while also estimating the source parameters simultaneously (in real observations, other considerations such as accuracy of gain calibration come into play (Natarajan et al., 2017)).

Applicable to problems in astrometry and geodesy.

Simulations for Astrometry (with Huib Jan van Langevelde)

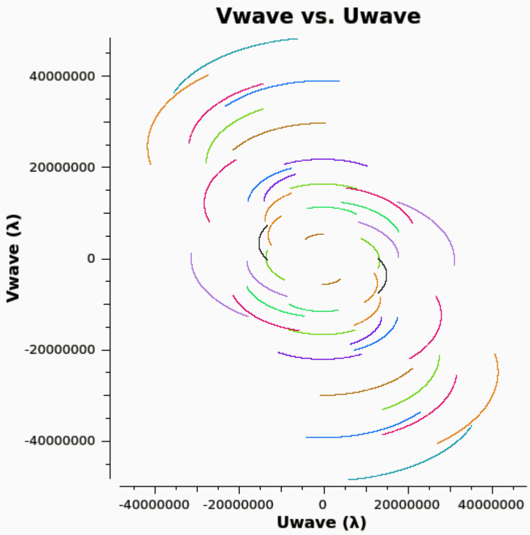

Details of the simulation:

- 7 EVN stations.
- Offset point source ($\sim$ 1000 mas from centre).
- 10 s integration time (4 hours total obs time).
- Frequency of 6.7 GHz.
- Single channel of 20 kHz.
- SEFD-derived thermal noise.
- Station-based phase offsets.

Posterior Distributions

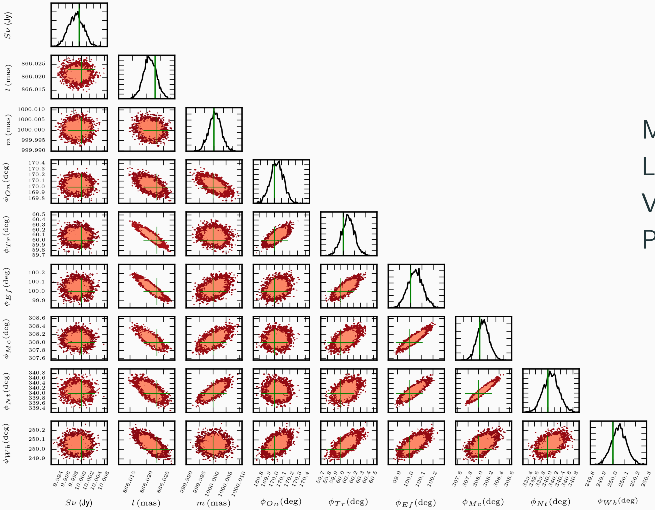

Main diagonal: 1-D posteriors

Lower triangle: 2-D correlations

Vertical green lines: simulated values

Parameters plotted:

- Flux Density, S_ν
- Position, (l, m)
- Phase offsets, ϕ_p

Next Steps...

Currently, time-variable delays (and other gain-terms) are handled by analysing solution interval chunks of data independently.

More complex source structures such as rings and multiple Gaussians need to be accounted for.

MULTINEST can handle only a few tens of parameters (~ 30) efficiently and execution times are high for large data sets: $\sim$ 15-20 hours to estimate 30 parameters for 12000 2×2 complex visibilities with a Tesla K40 GPU (2880 CUDA cores).

POLYCHORD looks promising for higher-dimensional models; some of the aforementioned tests were repeated using POLYCHORD (with MPI parallelisation), which brought down the execution time down to 30 minutes to 2 hours, depending on the required accuracy.

Newer version of MONTBLANC (under testing) can distribute model computation between multiple GPUs.

Questions?

References

Blecher, T., Deane, R., Bernardi, G., & Smirnov, O. (2017). MEQSILHOUETTE: a mm-VLBI observation and signal corruption simulator. *Monthly Notices of the Royal Astronomical Society*, 464, 143–151.

Cotton, W. D. (1995). Fringe Fitting. In J. A. Zensus, P. J. Diamond, & P. J. Napier (Eds.), *Very Long Baseline Interferometry and the VLBA*, volume 82 of *Astronomical Society of the Pacific Conference Series* (pp. 189).

Doeleman, S., Agol, E., Backer, D., Baganoff, F., Bower, G. C., Broderick, A., Fabian, A., Fish, V., Gammie, C., Ho, P., Honman, M., Krichbaum, T., Loeb, A., Marrone, D., Reid, M., Rogers, A., Shapiro, I., Strittmatter, P., Tilanus, R., Weintroub, J., Whitney, A., Wright, M., & Ziurys, L. (2009). Imaging an Event Horizon: submm-VLBI of a Super Massive Black Hole. In *astro2010: The Astronomy and Astrophysics Decadal Survey*, volume 2010 of *ArXiv Astrophysics e-prints*.

Feroz, F. & Hobson, M. P. (2008). Multimodal nested sampling: an efficient and robust alternative to MCMC methods for astronomical data analysis. *Monthly Notices of the Royal Astronomical Society*, 384, 449–463.

Handley, W. J., Hobson, M. P., & Lasenby, A. N. (2015). POLYCHORD: nested sampling for cosmology. *Monthly Notices of the Royal Astronomical Society*, 450, L61–L65.

Natarajan, I., Paragi, Z., Zwart, J., Perkins, S., Smirnov, O., & van der Heyden, K. (2017). Resolving the blazar CGRaBS J0809+5341 in the presence of telescope systematics. *Monthly Notices of the Royal Astronomical Society*, 464, 4306–4317.

Perkins, S., Marais, P., Zwart, J., Natarajan, I., Tasse, C., & Smirnov, O. (2015). Montblanc: GPU accelerated radio interferometer measurement equations in support of Bayesian inference for radio observations. *Astronomy and Computing*, 12, 73–85.

Schwab, F. R. & Cotton, W. D. (1983). Global fringe search techniques for VLBI. *The Astronomical Journal*, 88, 688–694.

Thompson, A. R., Moran, J. M., & George W. Swenson, J. (2017). *Interferometry and Synthesis in Radio Astronomy*. Wiley-Interscience, 3rd edition.